Journal of Alloys and Compounds 509 (2011) 7943–7947

Contents lists available at ScienceDirect

Journal of Alloys and Compounds

journal homepage: www.elsevier.com/locate/jallcom

Solvothermal synthesis of monodisperse ultrasmall cubic-structure Ba_2YbF_7 nanocrystals with intense upconversion

Xu Changfu[a,b], Ma Mo[a,b], Zeng Songjun[a,b], Ren Guozhong[a,b], Yang Liwen[a,c], Yang Qibin[a,b,*]

[a] Key Laboratory of Low Dimensional Materials &Application Technology of Ministry of Education, Xiangtan University, Xiangtan 411105, China
[b] Institute of Modern Physics, Faculty of Material & Photoelectronic Physics, Xiangtan university, Xiangtan 411105, China
[c] Laboratory for Quantum Engineering and Micro-Nano Energy Technology and Faculty of Materials and Optoelectronic Physics, Xiangtan University, Hunan 411105, China

ARTICLE INFO

Article history:
Received 15 April 2011
Received in revised form 6 May 2011
Accepted 12 May 2011
Available online 19 May 2011

Keywords:
Ba_2YbF_7 nanocrystal
Ultrasmall
Upconversion
Monodisperse

ABSTRACT

A series of monodisperse ultrasmall Ba_2YbF_7 nanocrystals with intense upconversion emission were synthesized via a facile solvothermal method by using oleic acid as capping ligands. X-ray diffraction (XRD) and transmission electron microscopy (TEM) assays revealed that the as-synthesized Ba_2YbF_7 nanocrystals are of cubic structure, rather than the reported tetragonal structure. The cell parameter of the particles is 5.918 Å. The Er^{3+} or Tm^{3+} doped Ba_2YbF_7 nanocrystals with the size of sub-10 nm can give an intense upconversion emission under the 980 nm laser excitation and the upconversion processes were discussed. The Ba_2YbF_7 nanocrystals show a potential application as a bioimaging agent.

1. Introduction

Monodisperse ultrasmall upconversion rare earth (Re) compound nanocrystals have showed actual and potential applications in bioimaging [1–3]. Compared to the traditional fluorescent dyes and semiconductor quantum dots, upconversion nanocrystals possess advantages such as excellent photostability, low photodamage and absence of autofluorescence background, and consequently, they can give an intense near-infrared (NIR) emission and can also be excited by NIR [4–8]. For example, Cohen [9] and Hyeon co-workers [10] present single $NaYF_4$ and $NaGdF_4$ nanocrystal possess ideal upconversion and photostability properties for single-molecule imaging. Therefore, great efforts have been devoted to find new host materials which have high efficient upconversion emission and to develop many protocols to synthesize monodisperse upconversion nanocrystals with uniform and ultrasmall size [11–13]. Yan developed the thermal chemical decomposition method, by which, ReF_3, $NaReF_4$, ReOF monodisperse nanocrystals with high quality can be synthesized [14]. Li and co-workers had prepared many kinds of high quality upconversion nanocrystals with the solvothermal method by using oleate as capping ligands [15]. Although these two protocols can be used to synthesize highly efficient upconversion nanocrystals with ultrasmall and uniform size, by contrast, the solvothermal method is more economic, "green" and convenient. With both protocols, series of $NaReF_4$ with different sizes and shapes, which often are of hexagonal and cubic structures, have been systematically researched, synthesized and applied in many fields [16–23]. In addition, the hexagonal structure $NaYF_4$ is recognized as highest efficient upconversion host material and presents highly photostability. However, the size of all monodisperse $NaReF_4$ nanocrystals is difficult to be tuned down to the size of sub-10 nm for the bioimaging of cellular apparatus [24]. Generally, the size of nanocrystals obviously affects the upconversion emission intensity [25,26] and the upconverted efficiency falls rapidly as the size of nanocrystals decreases. Until now, it has not been reported that ultrasmall upconversion nanocrystals can be used in the staining of cytoskeleton fibers which were definitely displayed by quantum dots with the size of 4–10 nm in diameter [24]. In fact, with the same doping conditions, Lin proved $BaGdF_5$ possessed higher efficiency than β-$NaYF_4$ when the size of nanocrystals was down to sub-10 nm [27].

The use of upconversion nanocrystals which surface is conjugated with organic or biological molecules will be extended to the fields of sensing, cellular targeting, bioimaging and other applications. So, it is necessary to find new host materials with enough-small size which can realize high efficient upconversion. At the same time, these new host materials can be synthesized as monodisperse, ultrasmall and uniform-size nanocrystals. In this work, a series of monodisperse ultrasmall Ba_2YbF_7 nanocrystals with the size of sub-10 nm were synthesized via the solvothermal method. The as-synthesized Ba_2YbF_7 nanocrystals are of cubic structure rather than the reported tetragonal structure

* Corresponding author.
E-mail address: yangqibin02002@yahoo.com.cn (Y. Qibin).

0925-8388/$ – see front matter © 2011 Elsevier B.V. All rights reserved.
doi:10.1016/j.jallcom.2011.05.045

(JCPDS 41-0823). Intense upconversion emission can be observed in these Er^{3+} or Tm^{3+} doped Ba_2YbF_7 nanocrystals with different doping conditions under a 980 nm laser excitation. To best of our knowledge, we have not found any reports about the upconversion property of Ba_2YbF_7 nanocrystals, so we believe that Ba_2YbF_7 would be a nice candidate agent for bioimaging.

2. Experimental and characterization

2.1. Synthesis of Ba_2YbF_7 nanocrystals

All reagents were purchased from Sinapharm Chemical Reagent Co., Ltd. and of analytical grade without further purification, but Re oxides purity is higher than 99.99%. Re oxides were dissolved in nitric acid at elevated temperature to form 0.5 M Re nitride solution, and then the concentration of partly $Tm(NO_3)_3$ and $Er(NO_3)_3$ were diluted to 0.05 M as doping reagents. Ba_2YbF_7 nanocrystals were synthesized by the following solvothermal method, which was used to synthesize $BaYF_5$ nanocrystals in our previous reports [17,18,28]. In a typical synthesis protocol, 2 ml aqueous solution containing 0.6 g NaOH, 10 ml alcohol and 20 ml oleic acid was added into a beaker by turn under stirring to form transparent homogeneous solution. Then, 3 ml $Ba(NO_3)_2$ (1 mmol) and 0.5 mmol $Yb(NO_3)_3$ or $Er(NO_3)_3$ aqueous solutions were introduced into the former solution. Finally, 2 ml NH_4F (4 mmol) aqueous solution were added to the solution under vigorous stirring. The resulting mixture was vigorously stirred for another 10 min to form a homogeneous colloidal solution. Then it was transferred into a 50 ml stainless Teflon-lined autoclave sealed, and kept at 220 °C for 24 h. After the reaction, the autoclave was moved out from the furnace and cooled down to the room temperature naturally. The products deposited at the bottom of the Teflon vessel were collected and washed with ethanol and water several times to remove other remnants, and then dried at 70 °C for 24 h or more time. With this method, a series of Er^{3+} or Tm^{3+} doped Ba_2YbF_7 nanocrystals were synthesized.

2.2. Structure and upconversion characterization

The phase and structure were identified with a D/Max 8550 X-ray power diffraction apparatus with Cu Kα radiation (λ = 1.5406 Å) at 40 kV and 40 mA. Analysis of X-ray diffraction (XRD) data were performed with MDI Jade 6.0 software. The morphologies and structure of the as-synthesized nanocrystals were characterized by transmission electron microscopy (TEM) (JEM-2100) at 200 kV equipped with an Oxford instrument energy dispersive X-ray spectroscopy (EDS) system. The samples for the TEM and HRTEM assays were redispersed in cyclohexane and ultrasonicated to produce a well-dispersed suspension, and then one drop of this suspension was placed on a copper grid covered with hollow carbon film for TEM characterization. Upconversion photoluminescence was recorded by an R-500 fluorescence spectrophotometer under the excitation of a 980 nm laser. The digital photographs of Ba_2YbF_7 nanocrystals with photoluminescence property dissolved in cyclohexane were taken by a digital camera (Nikon D4000). All of these measures were performed at room temperature.

3. Results and discussion

3.1. Structure and shape of the as-synthesized nanocrystals

The phase compositions of the as-synthesized nanocrystals were identified by XRD. The typical XRD patterns of the as-synthesized nanocrystals of Ba_2YbF_7, $Ba_2Yb_{0.998}Tm_{0.002}F_7$, $Ba_2Yb_{0.9}Er_{0.1}F_7$ and $Ba_2Yb_{0.8}Er_{0.2}F_7$ are shown in Fig. 1a–d, respectively. It can be seen that ten characteristic diffraction peaks appear at the positions of 2θ = 26.13, 30.25, 43.27, 51.21, 53.66, 62.81, 69.19, 71.25, 79.29 and 85.17° on the XRD pattern of Ba_2YbF_7 (Fig. 1a), respectively. Compared with that of the tetragonal structure Ba_2YbF_7 reported in the previous work (JCPDS 41-0823, S.G.: I, a = 4.202, c = 17.963 Å), many diffraction peaks are absent on the XRD pattern, and it is apparent that the crystal structure of the as-synthesized Ba_2YbF_7 nanocrystals in the present work exhibits higher symmetry in space group. It is found that the positions of the diffraction peaks of all the phases is matched to that of the Ba_2LaF_7 phase with the face-centered cubic (FCC) lattice (JCPDS 48-0099, cell parameter a = 6.088 Å), and thus it is supposed that the as-synthesized Ba_2YbF_7 nanocrystals may have the same structure as Ba_2LaF_7. To further verify it, EDS analysis was conducted on the sample, and the result reveals that the sample contains Ba, Yb and F. As shown in Fig. 2, besides copper and carbon come from the

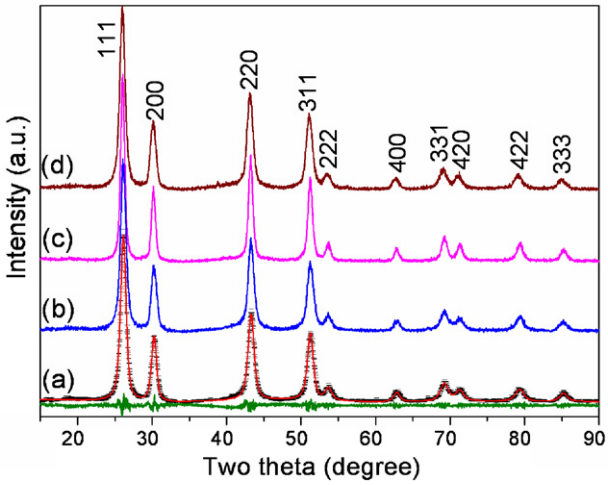

Fig. 1. XRD of cubic structure Ba_2YbF_7 nanocrystals reacted for 24 h: (a) Ba_2YbF_7 (The "–" are the raw XRD data and the overlapping red lines are calculated pattern. The olive curves at the bottom are the difference between the raw XRD data and the calculated data); b, $Ba_2Yb_{0.998}Tm_{0.002}F_7$; c, $Ba_2Yb_{0.9}Er_{0.1}F_7$; d, $Ba_2Yb_{0.8}Er_{0.2}F_7$. (For interpretation of the references to color in this figure legend, the reader is referred to the web version of the article.)

copper grid, the atom contents of Ba, Yb and F are 25.24, 14.45 and 60.31 at%, respectively, which are close to the formula of Ba_2YbF_7 as the difference originated from EDS measurement was considered. Moreover, the XRD data of the Ba_2YbF_7 nanocrystals are processed with Jade 6.0 software by taking the structure of cubic Ba_2LaF_7 as the model for WPF refinement. The calculated results and the XRD data, as well as the difference between them, are given in Fig. 1a. It can be seen that the calculated value are in good agreement with the XRD data with the difference of R = 10.02%. Therefore, it is believable that the as-synthesized nanocrystals are of face-centered cubic structure (S.G.: Fm-3m, cell parameter: a = 5.918 Å). Based on the above results, the cell parameters of two other Er^{3+} doped Ba_2YbF_7 nanocrystals were determined to be 5.920 Å for $Ba_2Yb_{0.9}Er_{0.1}F_7$ and 5.929 Å for $Ba_2Yb_{0.8}Er_{0.2}F_7$, respectively. It is found that the cell parameter increases as the Er^{3+} content increases since the radius of Er^{3+} is bigger than that of Yb^{3+}. In addition, the cell parameter of $Ba_2Yb_{0.998}Tm_{0.002}F_7$ is calculated to be 5.916 Å, which is close to that of Ba_2YbF_7.

Moreover, it can be seen that the diffraction peaks are obviously widened due to the small-size effect of nanocrystals. The average size of the as-synthesized nanocrystals can be estimated by using

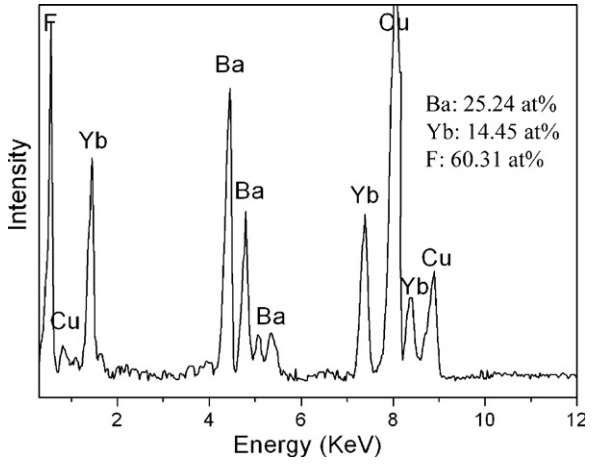

Fig. 2. Energy dispersive X-ray spectroscopy (EDS) analyses of Ba_2YbF_7 nanocrystals, revealing the presence of component elements.

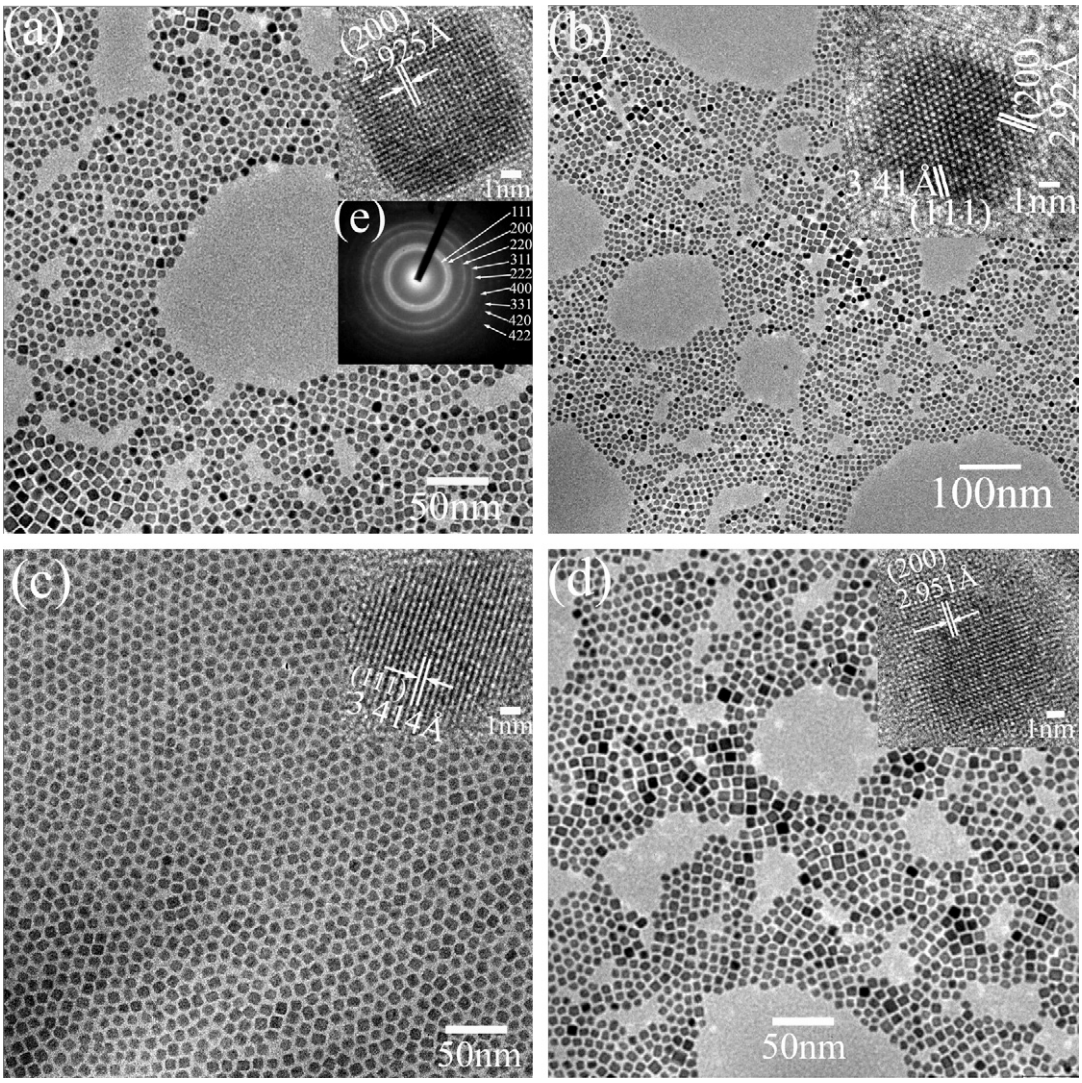

Fig. 3. TEM images of as-synthesized oleate capped nanocrystals: (a) Ba_2YbF_7; (b) $Ba_2Yb_{0.998}Tm_{0.002}F_7$; (c) $Ba_2Yb_{0.9}Er_{0.1}F_7$; (d) $Ba_2Yb_{0.8}Er_{0.2}F_7$; (e) the inset in a corresponding to the SAED image of Ba_2YbF_7. The insets in the top right corner of each TEM images are their corresponding high resolution TEM images.

Scherrer equation as follows: $D = K\lambda/\beta\cos\theta$, where λ is the X-ray wavelength (0.15406 nm), β is the full-width at half-maximum, θ is the diffraction angle, and K is a constant (0.89). The particle sizes of the as-synthesized Ba_2YbF_7 and Tm^{3+} or Er^{3+} doped Ba_2YbF_7 nanocrystals are estimated to be 6.3 nm for Ba_2YbF_7, 7.6 nm for $Ba_2Yb_{0.998}Tm_{0.002}F_7$, 6.7 nm for $Ba_2Yb_{0.9}Er0.1F_7$ and 7.4 nm for $Ba_2Yb_{0.8}Er_{0.2}F_7$, respectively. The results indicate that the Er^{3+} or Tm^{3+} dopant concentration has no obvious influence on the size of the Ba_2YbF_7 nanocrystals.

Insights in the microstructure of the sample can be obtained by further analysis of TEM and HRTEM assays. Fig. 3a–d showed the TEM and HRTEM images of Ba_2YbF_7, $Ba_2Yb_{0.998}Tm_{0.002}$, F_7, $Ba_2Yb_{0.9}Er_{0.1}F_7$, and $Ba_2Yb_{0.8}Er_{0.2}F_7$ particles, respectively. It can be seen that all the as-synthesized nanocrystals are high uniform, well dispersed, and self-assemble into two-dimensional order array. The sizes of nanocrystals can be measured from Fig. 3, which are in good agreement with that calculated from the corresponding XRD pattern. The as-synthesized nanocrystals are in cubic or truncated-cubic shapes. The interplanar distances calculated with the diameter of inner seven SAED rings (inset in Fig. 3a) are 3.42, 2.96, 2.11, 1.79, 1.72, 1.48 and 1.36 Å, which can be assigned to (1 1 1), (2 0 0), (2 2 0), (3 1 1), (2 2 2), (4 0 0) and (3 3 1) lattice planes of the face-centered cubic structure Ba_2YbF_7, respectively. High resolution TEM images reveal that the lattice fringes for these three samples are 2.925 Å for (2 0 0) planes of Ba_2YbF_7, 3.41 and 2.92 Å for (1 1 1) and (2 0 0) planes of $Ba_2Yb_{0.998}Tm_{0.002}F_7$, 3.414 Å for (1 1 1) planes of $Ba_2Yb_{0.9}Er_{0.1}F_7$ and 2.953 Å for (2 0 0) planes of $Ba_2Yb_{0.8}Er_{0.2}F_7$. The high resolution TEM images also prove the lattice parameters increase as the Er^{3+} content increases for Er^{3+} has a bigger radius than Yb^{3+}. It is worthy noted that high concentration doping does not change the phase structure of Ba_2YbF_7 nanocrystals and has no obvious effect on the shape and size.

3.2. Upconversion emission of the as-synthesized Ba_2YbF_7 nanocrystals

Intense upconversion emission can be observed in Er^{3+} or Tm^{3+} doped Ba_2YbF_7 nanocrystals. Fig. 4a–d provides the upconversion emission spectra of the as-synthesized $Ba_2Yb_{1-x}Er_xF_7$ (a, $x = 0.02$; b, $x = 0.04$; c, $x = 0.10$; d, $x = 0.20$; e, the inset is the digital photograph of $Ba_2Yb_{0.98}Er_{0.02}F_7$) nanocrystals with different Er^{3+} dopant concentrations under the excitation of a 980 nm laser. Obviously, the yellow color emission is originated from the inner-4f electron energy level transitions of Er^{3+} and the emission intensity changes as the Er^{3+} content variation. Minor Er^{3+} doping can enhance the emission intensity of Ba_2YbF_7 remarkably and the highest emission intensity can be obtained in $Ba_2Yb_{0.96}Er_{0.04}F_7$. More Er^{3+} doping will impair the emission intensity for that the high con-

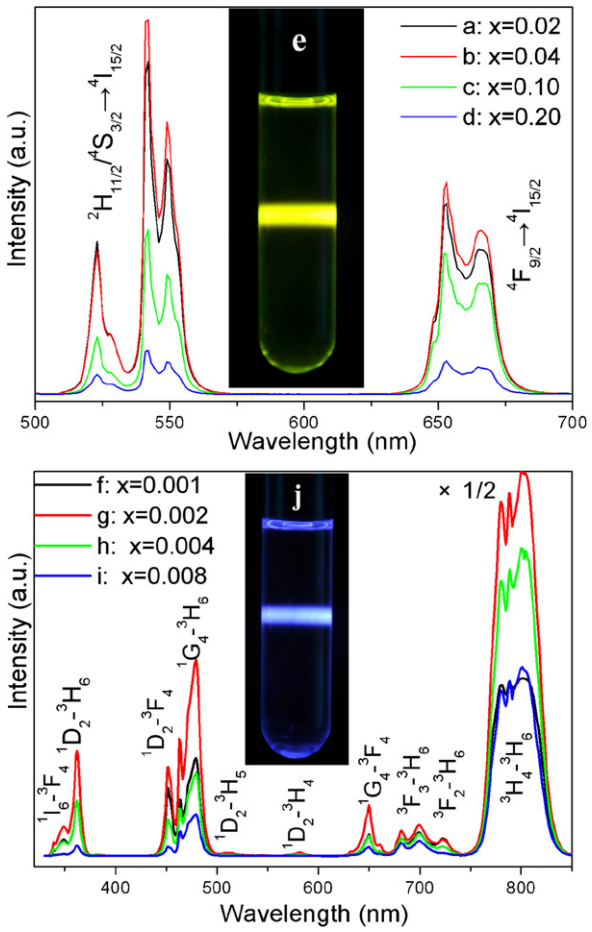

Fig. 4. Upconversion emission of as-synthesized Ba_2YbF_7 nanocrystals: $Ba_2Yb_{1-x}Er_xF_7$ (a) $x = 0.02$; (b) $x = 0.04$; (c) $x = 0.10$; (d) $x = 0.20$) and $Ba_2Yb_{1-x}Tm_xF_7$ (f) $x = 0.001$; (g) $x = 0.002$; (h), $x = 0.004$; (i) $x = 0.008$). The insets are the digital photographs of $Ba_2Yb_{0.98}Er_{0.02}F_7$ (e) and $Ba_2Yb_{0.998}Tm_{0.002}F_7$ (j) under the excitation of 980 nm laser with the output power of 30 W/cm^2.

centration doping of Er^{3+} weakens the sensitization of Yb^{3+} and deduces the concentration quenching. Two main emission bands exist in Er^{3+} doped Ba_2YbF_7 nanocrystals. The green band centered at 523, 542 and 549 nm originates from transitions of Er^{3+}: $^2H_{11/2}/^4S_{3/2} \rightarrow {}^4I_{15/2}$, and the red band centered at 652 and 665 nm can be ascribed to the transition of Er^{3+}: $^4F_{9/2} \rightarrow {}^4I_{15/2}$. It is obvious that excessive Er^{3+} does not favor the upconversion efficiency.

Intense upconversion emission can be realized in Ba_2YbF_7 nanocrystals at different Tm^{3+} dopant concentrations under the excitation of a 980 nm laser. The emission spectra are given in Fig. 4f–i: $Ba_2Yb_{1-x}Tm_xF_7$ (f, $x = 0.001$; g, $x = 0.002$; h, $x = 0.004$; i, $x = 0.008$; j, the inset is the digital photograph of $Ba_2Yb_{0.998}Tm_{0.002}F_7$). Similar to the Er^{3+} doping, just minor Tm^{3+} dopant can realize intense upconversion emission. When Tm^{3+} dopant concentration increased to 0.002, the highest emission intensity was gotten. It is noted that intense ultraviolet emission band can be observed. In fact, there are four luminescent bands ranging from ultraviolet to near-infrared originated from the inner 4f electron energy levels transitions of Tm^{3+}. The ultraviolet emission band centered at 348 and 360 nm can be attributed to the transitions of $^1I_6 \rightarrow {}^3F_4$ and $^1D_2 \rightarrow {}^3H_6$. The blue emission band centered at 452 and 476 nm can be ascribed to the transitions of $^1D_2 \rightarrow {}^3F_4$ and $^1G_4 \rightarrow {}^3H_6$. The transitions of $^1G_4 \rightarrow {}^3F_4$, $^3F_2 \rightarrow {}^3H_6$ and $^3F_3 \rightarrow {}^3H_6$ induces the red emission centered at 648, 696, 723 nm. The predominant near-infrared emissions centered at 800 nm are due to the transition of $^3H_4 \rightarrow {}^3H_6$. In addition, very weak green and yellow upconversion emission bands, which are centered at 511 and 581 nm respectively, can be observed in $Ba_2Yb_{0.998}Tm_{0.002}F_7$ nanocrystals. Compared to the blue emission, the red emission band (from 630 to 730 nm) is much weak in the visible wave band, so these four Tm^{3+} doped Ba_2YbF_7 nanocrystals present blue emission by naked eyes under the excitation of a 980 nm laser.

Intense upconversion can be observed in Er^{3+} or Tm^{3+} doped Ba_2YbF_7 nanocrystals, which means the high Yb^{3+} concentration in Ba_2YbF_7 did not lead concentration quenching. When Yb^{3+} is used as sensitizer for many host materials, the doping concentration is often about 20% to get best upconversion efficiency. In fact, Yb^{3+} works as sensitizer and composition in many host materials such as $NaYbF_4$ [18] and $Al_5Yb_3O_{12}$ [29,30].

These Ba_2YbF_7 nanocrystals can be redispersed in cyclohexane to form the transparent colloid solution, from which intense upconversion emission can be observed by naked eyes under the excitation of a 980 nm laser with the output power of 30 W/cm^2 and taken by the digital camera (Fig. 4e and j). All of these facts prove that Ba_2YbF_7 is a new type of nice upconversion host material which will be a potential candidate agent for bioimaging applications.

In order to understand the process of emissions, the dependence of emission intensity I_{up} of Er^{3+} or Tm^{3+} doped Ba_2YbF_7 nanocrystals on the infrared excitation power P were measured. As shown in Fig. 5 by log–log plots, I_{up} is proportional to the Nth power of P: $I_{up} \propto P^N$, where N is the order of multi-photon transitions, a number of infrared quanta absorbed per one photon emission. Under the 980 nm laser excitation, the slopes of Er^{3+} doped Ba_2YbF_7 nanocrystals are obtained to be $N = 1.91$, 1.73 and 1.94 corresponding to 523, 542 and 652 nm emissions, respectively. That means two-photon process for 523, 542 and 652 nm emission. For Tm^{3+} doped Ba_2YbF_7 nanocrystals, the values of N are 4.70, 3.78, 3.66, 2.96, 2.51, 1.86 and 1.60 at 349, 362, 452, 479, 650, 699 and 808 nm emissions, indicating that 5, 4, 4, 3, 3, 2 and 2 photons are needed, respectively.

For Yb^{3+} has much bigger absorption section than Er^{3+} or Tm^{3+} under the excitation of the 980 nm laser, high efficient upconversion processes of Er^{3+} or Tm^{3+} doped Ba_2YbF_7 nanocrystals are originated from the sensitization of Yb^{3+} ions [31]. Fig. 6 gives the schemes of energy transfer processes of (a) $Yb^{3+} \rightarrow Er^{3+}$ and (b) $Yb^{3+} \rightarrow Tm^{3+}$ under the excitation of 980 nm laser. As shown in Fig. 6a, Er^{3+} is pumped to $^4I_{11/2}$ level by the energy transfer from Yb^{3+}, and then part nonradiatively relaxes to next lower level $^4I_{13/2}$. The populations of $^4F_{7/2}$ and $^4F_{9/2}$ levels are formed by the successive energy transfer from Yb^{3+}. The electrons populated on $^4F_{7/2}$ level nonradiatively relax to next lower levels $^2H_{11/2}$ and $^4S_{3/2}$ [32]. So, the emissions of Er^{3+} doped Ba_2YbF_7 nanocrystals can be obtained by the following processes.

For 652 nm emission: $^4I_{15/2}$ $(Er^{3+}) + {}^2F_{5/2}$ $(Yb^{3+}) \rightarrow {}^4I_{11/2}$ $(Er^{3+}) + {}^2F_{7/2}$ (Yb^{3+}), $^4I_{11/2}$ $(Er^{3+}) \rightarrow {}^4I_{13/2}$ (Er^{3+}) + phonons, $^4I_{13/2}$ $(Er^{3+}) + {}^2F_{5/2}$ $(Yb^{3+}) \rightarrow {}^4F_{9/2}$ $(Er^{3+}) + {}^2F_{7/2}$ (Yb^{3+}), $^2F_{9/2}$ $(Er^{3+}) \rightarrow {}^4I_{15/2}$ (Er^{3+}) + a photon (652 nm);

For 523 and 542 nm emissions: $^4I_{15/2}$ $(Er^{3+}) + {}^2F_{5/2}$ $(Yb^{3+}) \rightarrow {}^4I_{11/2}$ $(Er^{3+}) + {}^2F_{7/2}$ (Yb^{3+}), $^4I_{11/2}$ $(Er^{3+}) + {}^2F_{5/2}$ $(Yb^{3+}) \rightarrow {}^4F_{7/2}$ $(Er^{3+}) + {}^2F_{7/2}$ (Yb^{3+}), $^4F_{7/2}$ $(Er^{3+}) \rightarrow {}^2H_{11/2}$ or $^4S_{3/2}$ + phonons, $^2H_{11/2}$ or $^4S_{3/2} \rightarrow {}^4I_{15/2}$ (Er^{3+}) + a photon (523 or 542 nm).

Fig. 6b has shown the population and upconversion processes Tm^{3+} doped Ba_2YbF_7 nanocrystals. The possible UC mechanisms to populate the excited levels might be realized via the multiple phonon-assisted energy transfer processes from Yb^{3+} ions to Tm^{3+} ions as follows: $^2F_{5/2}$ $(Yb^{3+}) + {}^3H_6$ $(Tm^{3+}) \rightarrow {}^3H_5$ $(Tm^{3+}) + {}^2F_{7/2}$ $(Yb^{3+}) \sim {}^3F_4$ (Tm^{3+}) + multiphonon relaxation, $^2F_{5/2}$ $(Yb^{3+}) + {}^3F_4$ $(Tm^{3+}) \rightarrow {}^3F_2/{}^3F_3$ $(Tm^{3+}) + {}^2F_{7/2}$ $(Yb^{3+}) \sim {}^3H_4$ (Tm^{3+}) + multiphonon relaxation, $^2F_{5/2}$ $(Yb^{3+}) + {}^3H_4$ $(Tm^{3+}) \rightarrow {}^1G_4$ $(Tm^{3+}) + {}^2F_{7/2}$ (Yb^{3+}), $^3H_4$ $(Tm^{3+}) + {}^3F_3$ $(Tm^{3+}) \rightarrow {}^1D_2$ $(Tm^{3+}) + {}^3H_6$ (Tm^{3+}), $^2F_{5/2}$ $(Yb^{3+}) + {}^1D_2$ $(Tm^{3+}) \rightarrow {}^3P_{1,2}$ $(Tm^{3+}) + {}^2F_{7/2}$ $(Yb^{3+}) \sim {}^1I_6$ (Tm^{3+}) + multiphonon relaxation. Then, the transitions from the

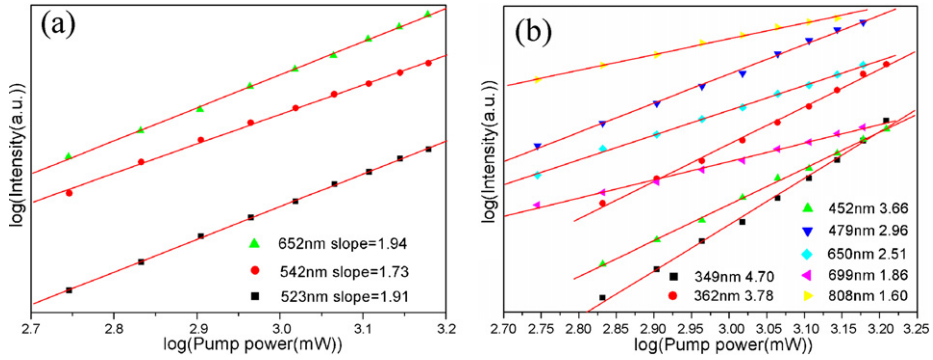

Fig. 5. Double-logarithmic plots of excitation power dependent upconversion emission intensity of (a) Er^{3+} and (b) Tm^{3+} doped Ba_2YbF_7 nanocrystals under the excitation of a 980 nm laser.

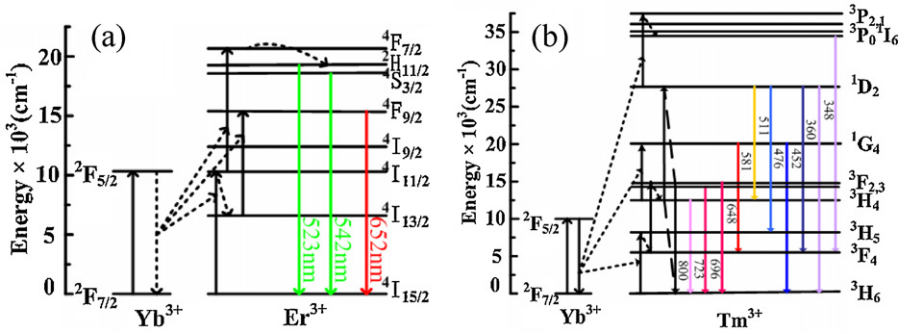

Fig. 6. Schemes of energy transfer processes of (a) $Yb^{3+} \rightarrow Er^{3+}$ and (b) $Yb^{3+} \rightarrow Tm^{3+}$ under the excitation of 980 nm laser.

excited state levels to lower and ground states lead the emissions of Tm^{3+}: $^1I_6 \rightarrow {}^3F_4$ + photon (348 nm), $^1D_2 \rightarrow {}^3H_6$ + photon (360 nm), $^1D_2 \rightarrow {}^3F_4$ + photon (452 nm), $^1G_4 \rightarrow {}^3H_6$ + photon (476 nm), $^1D_2 \rightarrow {}^3F_5$ + photon (511 nm), $^1D_2 \rightarrow {}^3F_4$ + photon (581 nm), $^1G_4 \rightarrow {}^3F_4$ + photon (648 nm), $^3F_2 \rightarrow {}^3H_6$ (696 nm), $^3F_3 \rightarrow {}^3H_6$ (723 nm) and $^3H_4 \rightarrow {}^3H_6$ (800 nm).

4. Conclusions

Ultrasmall monodisperse Ba_2YbF_7 nanocrystals with the size of sub-10 nm were synthesized via solvothermal method. TEM and XRD assays revealed that Ba_2YbF_7 nanocrystals are of cubic structure and their cell parameter is 5.918 Å. The as-synthesized Er^{3+} or Tm^{3+} doped Ba_2YbF_7 nanocrystals possess nice photoluminescent property and the upconversion emission intensity can be tuned by controllable doping concentration. Especially, the Tm^{3+} doped Ba_2YbF_7 nanocrystals have intense upconversion emission in the range from NIR to the ultraviolet under the 980 nm laser excitation. Our results prove monodisperse ultrasmall Ba_2YbF_7 nanocrystals have great potential in bioimaging applications.

Acknowledgement

This work was supported by the grants from National Natural Science Foundation of China (no.10874144).

References

[1] M. Nyk, R. Kumar, T.Y. Ohulchanskyy, E.J. Bergey, P.N. Prasad, Nano Lett. 8 (2008) 3834.
[2] J. Zhou, M. Yu, X. Zhang, X. Zhu, Z. Wu, D. Wu, F.Y. Li, Biomaterials 32 (2011) 1148.
[3] F. Wang, X.G. Liu, Chem. Soc. Rev. 38 (2009) 976.
[4] R. Kumar, M. Nyk, T. Ohulchanskyy, C. Flask, P. Prasad, Adv. Funct. Mater. 19 (2009) 853.
[5] Y. Park, J. Kim, K. Lee, K. Jeon, H. Na, J. Yu, H. Kim, N. Lee, S. Choi, S. Baik, H. Kim, S. ParK, B. Park, Y. Kim, S. Lee, S. Yoon, I. Song, W. Moom, Y. Suh, T. Hyeon, Adv. Mater. 21 (2009) 4467.
[6] L. Cheng, K. Yang, M. Shao, S.T. Lee, Z. Liu, J. Phys. Chem. C 115 (2011) 2686.
[7] F. Wang, D. Banerjee, Y.S. Liu, X.Y. Chen, X.G. Liu, Analyst 135 (2010) 1839.
[8] H.S. Mader, P. Kele, S.M. Saleh, O.S. Wolfbeis, Curr. Opin. Chem. Biol. 14 (2010) 582.
[9] S.W. Wu, G. Han, D. Milliron, S. Aloni, V. Altoe, D.V. Talapin, B.E. Cohen, P.J. Schuck, Proc. Natl. Acad. Sci. 106 (2009) 10917.
[10] Y. Park, J.H. Kim, K.T. Lee, K.S. Jeon, H.B. Na, J.H. Yu, H.M. Kim, N. Lee, S.H. Choi, S. Baik, H. Kim, S.P. Park, B.J. Park, Y.W. Kim, S.H. Lee, S.Y. Yoon, I.C. Song, W.K. Moon, Y.D. Suh, T. Hyeon, Adv. Mater. 21 (2009) 4467.
[11] F. Zhang, Y. Shi, X. Sun, D. Zhao, G.D. Stuchy, Chem. Mater. 21 (2009) 5237.
[12] Y. Liu, D. Tu, H. Zhu, R. Li, W. Luo, X.Y. Chen, Adv. Mater. 22 (2010) 3266.
[13] F. Zhang, D.Y. Zhao, ACS Nano 3 (2009) 159.
[14] H.X. Mai, Y.W. Zhang, R. Si, Z.G. Yan, L.D. Sun, L.P. You, C.H. Yan, J. Am. Chem. Soc. 128 (2006) 6426.
[15] X. Wang, J. Zhuang, Q. Peng, Y.D. Li, Nature 437 (2005) 121.
[16] S. Schietinger, T. Aichele, H.Q. Wang, T. Nann, O. Benson, Nano Lett. 10 (2010) 134.
[17] S.J. Zeng, G. Ren, C.F. Xu, Q.B. Yang, CrystEngComm 13 (2011) 1384.
[18] S.J. Zeng, G. Ren, W. Li, C.F. Xu, Q.B. Yang, J. Phys. Chem. C 114 (2010) 10750.
[19] G.Y. Chen, T.Y. Ohulchanskyy, R. Kumar, H. Agren, P.N. Prasad, ACS Nano 6 (2010) 3136.
[20] J. Zhuang, L. Liang, H.H.Y. Sung, X. Yang, M. Wu, I.D. Williams, S. Feng, Q. Su, Inorg. Chem. 46 (2007) 5404.
[21] V.K. Komarala, Y.J. Wang, M. Xiao, Chem. Phys. Lett. 490 (2010) 189.
[22] L. Wang, X. Xue, H. Chen, D. Zhao, W. Qin, Chem. Phys. Lett. 485 (2010) 183.
[23] F. Wang, Y. Han, C.S. Lim, Y.H. Lu, J. Wang, J. Xu, H.Y. Chen, C. Zhang, M.H. Hong, X.G. Liu, Nature 463 (2010) 1061.
[24] X.Y. Wu, H.J. Liu, J.Q. Liu, K.N. Haley, J.A. Treadway, J.P. Larson, N.F. Ge, G. Peale, M.P. Bruchez, Nat. Biotechnol. 21 (2003) 41.
[25] A.X. Yin, Y.W. Zhang, L.D. Sun, C.H. Yan, Nanoscale 2 (2010) 953.
[26] F. Wang, J. Wang, X.G. Liu, Angew. Chem. Int. Ed. 49 (2010) 7456.
[27] D.M. Yang, C.X. Li, G.G. Li, M.M. Shang, X.J. Kang, J. Lin, J. Mater. Chem. 21 (2011) 5923.
[28] M. Ma, L. Yang, G. Ren, C.F. Xu, L. Lin, Q. Yang, J. Lumin. 131 (2011) 1482.
[29] C.F. Xu, L.W. Yang, H.L. Han, Y.Y. Zhang, P.K. Chu, Opt. Mater. 32 (2010) 1188.
[30] C.F. Xu, Q.B. Yang, G.Z. Ren, Y. Liu, J. Alloys Compd. 503 (2010) 82.
[31] P. jenouvrier, G. Boccardi, J. Fick, A.M. Jurdyc, M. Langlet, J. Lumin. 113 (2005) 291.
[32] S. Sivakumar, F.C.J.M. van Veggel, P.S. May, J. Am. Chem. Soc. 129 (2007) 620.